

See discussions, stats, and author profiles for this publication at: <https://www.researchgate.net/publication/307555926>

Tidal stream resource assessment in the Dover Strait (eastern English Channel)

Article in International Journal of Marine Energy · August 2016

DOI: 10.1016/j.ijome.2016.08.004

CITATIONS

7

READS

634

2 authors:



Maxime Thiébaut
France Energies Marées

17 PUBLICATIONS 34 CITATIONS

[SEE PROFILE](#)



Alexei Sentchev
Université du Littoral Côte d'Opale (ULCO)

55 PUBLICATIONS 451 CITATIONS

[SEE PROFILE](#)

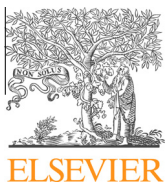
Some of the authors of this publication are also working on these related projects:



Project Pro-Tide, Interreg IVB NWE, Funding powerful solutions [View project](#)



Project THYMOTE - Tidal turbulence: modelling, field observations and tank experiments [View project](#)



Tidal stream resource assessment in the Dover Strait (eastern English Channel)



Maxime Thiébaut, Alexei Sentchev*

Univ. Littoral Côte d'Opale, Univ. Lille-1, CNRS, UMR 8187- LOG, Laboratoire d'Océanologie et de Géosciences, F 62930 Wimereux, France

ARTICLE INFO

Article history:

Received 25 April 2016

Revised 16 August 2016

Accepted 25 August 2016

Available online 26 August 2016

Keywords:

Tidal stream resource

Tidal flow asymmetry

VHF radar

Dover Strait

ABSTRACT

A methodology of tidal flow resource assessment in the Dover Strait is presented. The resource assessment is performed using surface velocity time series recorded by Very High Frequency Radars (VHFR) and ADCP velocity measurements. Following the EMEC guideline, the major parameters of tidal flow conventionally used for tidal energy site screening are estimated and mapped. The combination of two sources of data allowed to characterize the current velocity variation in three spatial dimensions and in time, which increased confidence in hydrokinetic resource assessment from the radar data. Current velocities provided by the radars show strong spatial variation and fortnightly modulation. The most energetic area was found west of the Cape Gris Nez with the peak velocity of 2.5 m/s, mean velocity of 1 m/s, and spring tide average velocity of 1.4 m/s. Velocities exceeding 1 m/s are observed more than 50% of time there. Averaged velocity profiles derived from ADCP data were obtained for different stages of the tidal cycle and then approximated by a power law function. Using velocity time series provided by the radars and the power law velocity profiles, the power density time series in the surface and bottom layers were generated. The analysis of these data show that west of the Cape Gris Nez, the mean power density attains its maximum value 0.9 kW/m² in the surface layer and a peak value 5 kW/m². In the rest of the domain, the mean power density varies from 0.1 to 0.6 kW/m². The power density is found three times lower in the bottom layer. A three dimensional hydrodynamic model MARS-3D is used for comparison with experimental data. The model results are in good agreement with observations thus allowing the use of the model for assessing tidal stream resource in extended area.

© 2016 Elsevier Ltd. All rights reserved.

1. Introduction

Converting tidal current kinetic energy into electric power by in-stream tidal turbines became a real challenge since the last years. The world tidal energy potential (tidal range and tidal current) is of the order of 3 TW [1], thus offering a significant source of renewable energy. Sites with the biggest tidal stream potential are located on the northwest European shelf [2] and in particular in the English Channel [3]. Highly energetic areas such as Alderney Race, Bréhat Island region, Isle of Wight, and Dover Strait are considered as promising for tidal stream energy conversion [2]. Tidal projects are under development at several sites in France. In November 2015, the 0.5 MW Sabella D10 tidal turbine, installed in the Fromveur Strait, became the first marine current turbine to supply electricity to national power grid. In January 2016, the first of a total

* Corresponding author.

E-mail address: alexei.sentchev@univ-littoral.fr (A. Sentchev).

of three 0.5 MW turbine was installed at Paimpol-Bréhat demonstration site in France. Another project intends to explore in deep the French sector of Alderney Race (Raz Blanchard) and to prepare it for operational use. The Dover Strait is actually a subject of a study initiated by regional authorities in France. The new region Hauts-de-France has committed a sustainable development process with the purpose of dividing by 4 its gas emissions by 2050. Offshore wind and tidal energy represent a big potential for industrial exploitation. Tidal stream resource in the Dover Strait has been historically considered as non-negligible [3]. However there is no reliable estimate of a technically exploitable potential documented in scientific publications. The present study tends to get the knowledge on the resource available in this area.

Resource characterization is a first step toward site selection and turbine deployment planning [4]. Two approaches can be followed to quantify the tidal stream potential in the most efficient way: extensive field measurements and numerical modeling. Sometimes, both actions are combined together in order to increase the model performance or to help in interpretation of the experimental data [5,6].

The tidal flow potential can be quantified using a two-dimensional (2D) model. This is the more convenient, more simple and less expensive approach. Blunden and Bahaj [7] used the TELEMAC-2D modeling system to estimate the available resource at Portland Bill, UK. The model results were used to generate the tidal flow velocity time series over a large area and then to optimize the location of turbine arrays at the site. Xia et al. [8] used a 2D hydrodynamic model to assess the tidal current energy resource in the Severn Estuary, UK. Using a 2D finite element model (TIDE2D), Sutherland et al. [9] estimated the tidal stream potential as 1335 MW in the northwestern part of the Johnstone Strait, in Canada. Nowadays, three-dimensional (3D) models are routinely applied for tidal energy site assessment, resource quantification and studies of the impact of energy devices on local circulation and environment. Numerical simulations by Regional Ocean Modeling System (ROMS) were used to examine the tidal asymmetry in a promising site of Orkney Islands [10]. ROMS was also employed for evaluation of the wave influence on tidal stream energy resource [11] and for estimation of the tidal stream resource variability in the northwest European shelf seas [12].

Remotely sensed velocity observations or in situ velocity measurements at tidal energy sites represent a valuable alternative to modeling. The technique of field data acquisition is well established and currently used for resource characterization in many coastal ocean regions [5,13–15]. Acoustic Doppler current profiler (ADCP) is often the instrument of choice for fixed point or towed surveys. In the early studies (e.g. [16–18]), while the vessel steamed around a circuit, velocity profiles were recorded with sufficient frequency allowing to resolve the vertical structure of the tidal current and its spatial irregularities. More recently, Goddijn-Murphy et al. [5] used underway ADCP data to reconstruct the tidal flow patterns in the Inner Sound (Pentland Firth, UK). Sentchev and Yaremchuk [6] employed the optimal interpolation technique for reconstructing space–time evolution of the velocity field derived from towed ADCP surveys in the Boulogne harbour (English Channel).

But the most frequent are certainly velocity measurements by bottom mounted ADCPs – routinely used for assessing temporal variations of the tidal stream [13] and turbulent properties of the flow [19]. Turbulent kinetic energy, dissipation rate, Reynolds stress, and some other turbulent parameters can be retrieved from ADCP measurements [20,21].

In this study, a novel technique of tidal flow resource assessment is presented. It is based on the analysis of surface current velocity time series recorded by Very High Frequency Radar (VHFR) along the Opal coast, in the French sector of the Dover Strait [22]. Although the radar technology has been used in many oceanographic applications since more than 20 years (e.g. [23–25]), its efficiency for tidal energy resource assessment was demonstrated only recently [26]. The radar derived velocities were supplemented by current velocity profiles acquired by bottom mounted ADCPs in the study area. The radars allow continuous data acquisition of the surface current velocities over a large area at high spatial and time resolution. ADCP data provide information about velocity variation with depth which is fundamental for detailed tidal stream resource assessment. The knowledge of the three dimensional structure of a tidal flow in combination with the temporal variability of currents allows to assess the resource variability at a site from direct velocity measurements with a high degree of confidence. Results from the regional modeling in the Dover Strait are also used to support the estimation of the tidal stream potential derived from observations. A combination of different sources of data and numerical modeling allowed the detailed characterization of the tidal stream potential available in a region that was previously considered as promising for tidal energy conversion. The results of this research can be useful for decision makers and stakeholders for future development of renewable energy network at a regional scale.

2. Data and methods

2.1. Study site, environmental conditions and constraints

The study area is located in the Dover Strait (eastern English Channel), along the Opal coast of France (Fig. 1, right panel). The coastline is meridionally oriented with a large embayment in the central part (Boulogne harbour) and a number of small inlets and river estuaries. The water depth is less than 50 m throughout the domain. In the middle of the Dover Strait, there are sandbanks oriented in the alongshore direction.

Investigation of the physical processes which govern the circulation along the Opal coast has been performed using VHFR observations [22] and numerical modeling (e.g. [27–29]). The authors showed that the local hydrodynamics is by far dominated by tidal motions. Tidal wave propagating along the Opal coast determines the variability of the sea surface height

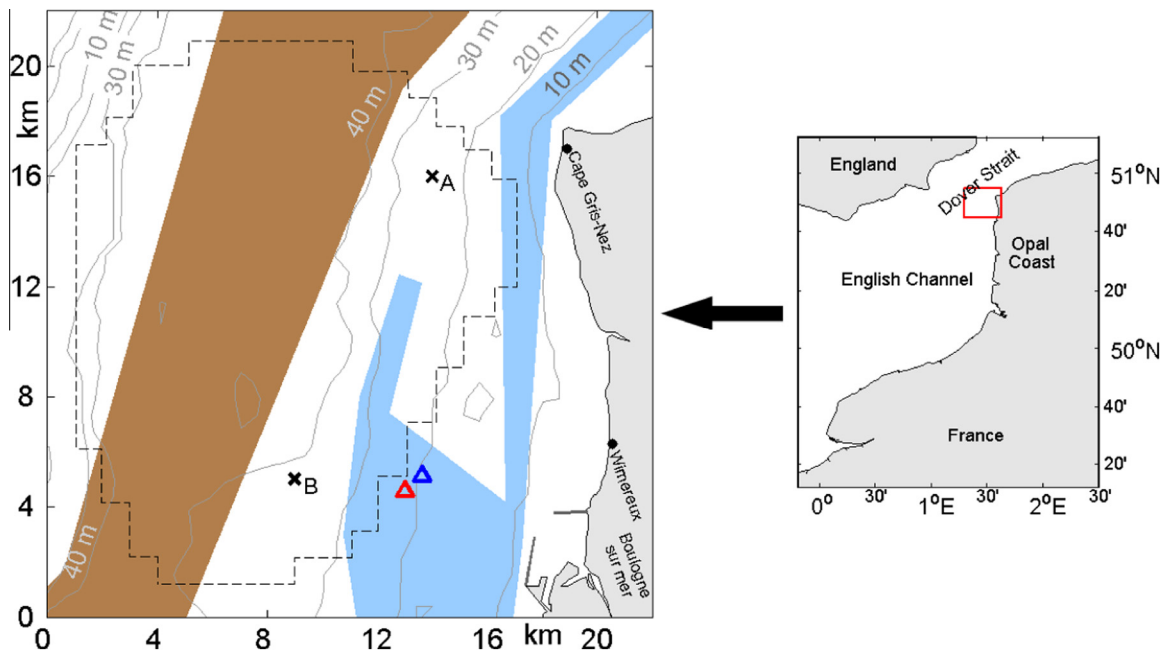


Fig. 1. Study area: off the Opal coast in the eastern English Channel (red square on the right panel). Radar sites are shown by black dots and the blue and red triangles denote the location of ADCPs in June 2008 and July 2009 respectively. Black crosses show locations A and B selected for a detailed analysis. The navigation way of vessels travelling northward is shown by brown shading. Blue shading matches the main fishing area. Contour interval of the bathymetry is 10 m (grey solid lines). Black dashed line indicates the radar coverage zone. Geographic names used in the text are also shown.

(SSH) and currents in the study area. The SSH in the Boulogne harbour (BLH) has a wide range of variations (4–9 m), whereas tidal current velocities have a typical magnitude of 1–1.5 m/s [30,31]. Currents are predominantly semi-diurnal with a pronounced fortnightly modulation due to the interference of the M_2 , S_2 and N_2 tidal constituents. A significant asymmetry of the sea-surface elevation curve reveals a contribution of higher order nonlinear harmonics (M_4 , MS_4). They also generate higher velocities during the flood flow compared to ebb flow [32].

Site assessment should take into account the environmental constraints relative to local economic activities. The Dover Strait is one of the busiest seaways in the world. More than 400 commercial vessels cross the strait daily. The traffic safety is a critical issue because of high risk of collision in the strait. The navigation way of vessels travelling northward is shown by brown shading in Fig. 1. The port of Boulogne is the biggest fishing port in France. Fishing is an important local economic activity and a large area is extensively exploited in the vicinity of the BLH (Fig. 1, blue shading). These constraints considerably limit the area suitable for marine renewable energy conversion.

Two particular locations, not affected by constraints mentioned above, are chosen for further detailed analysis of the technically exploitable potential in the study area: northern and southern sectors of the radar coverage zone (Fig. 1). The water depth ranges from 25 to 35 m there, which is favorable for tidal turbine installation [33].

2.2. VHFR data

In May–June 2003, two VHF radars were deployed to monitor surface currents off the French Opal coast for a 35-day period. One radar site was located on the Cape Gris Nez (hereafter Cape GN), 40 m above the sea level. The other radar was installed 12 km farther southward, in Wimereux (Fig. 1). The VHFR system “COSMER” [23] measures the current velocity in the surface layer (0.25 m thick). The radars, operating at frequencies 45 MHz and 47.8 MHz, were configured to provide measurements over a distance up to 25 km offshore at high spatial resolution: 600 m along beam and 10° azimuthal spacing, with time resolution of 20 min. The radial velocities measured by the two radars were interpolated on a regular grid with 1 km spacing by variational method with gap filling capability. As a result, one month long velocity time series were generated from May 1 to June 4, 2003. A detailed description of the experimental settings and methods of data processing of the radar network off the northern Opal coast can be found in [22].

2.3. ADCP data

ADCP measurements from two 1.2 MHz upward-looking four-beam broadband RDI ADCPs were used to supplement surface velocities provided by the radars. Both instruments were installed approximately 6 km west of the BLH at 18 m mean

depth (Fig. 1). The first ADCP was deployed from 1 to 4 July 2008, during spring tide, and the second one from 9 to 16 June 2009, covering the period of tide evolution from spring to neap. Velocities were recorded at 1 Hz in beam coordinates with 0.5 m vertical resolution, starting from 1 m above the bottom. The data from the surface 3 m thick layer were not considered in analyzed because of signal contamination by surface waves.

2.4. Numerical model

Three dimensional hydrodynamic model MARS-3D [34] was used to simulate the circulation in the Dover Strait. The model was configured at 140-m horizontal resolution with 20 sigma levels, vertically distributed such as to provide enhanced resolution near the surface and seabed. Forcing at the open boundaries was taken from a coarser resolution (1 km) regional model of the English Channel driven by the realistic winds, heat fluxes, and river runoff. The model employs a time-varying spatial grid in the vicinity of the coastline thus taking into account the wetting and drying phenomenon [35]. The time step of 30 s for both external and internal modes was used. Regional model validation was done by comparing model fields with tidal gage data in 20 ports, sea surface currents recorded by VHF radars. More details on the model configuration and validation can be found in [29]. The model was run for three 30-day-long periods, in May 2003, July 2008 and June 2009.

2.5. Data analysis

The principal component analysis (PCA) [36] was applied to quantify the tidal flow dynamics over the whole period of observations. As tidal currents are rotational, the current velocity vector evolving over a tidal cycle draws an ellipse. Parameters of synthesized ellipses, retrieved from the PCA, provide two major properties of tidal currents: direction and magnitude, and also indicate the tidal flow anisotropy. The latter is estimated as the ratio of eigenvalues of the velocity correlation tensor. This approach has a certain advantage over a frequently used harmonic analysis because it allows quantifying the total contribution of all tidal constituents to observed currents and assessing time-space variability of the flow. A rotary analysis technique [36] has been also applied to velocity time series in order to identify the ellipse polarization or the sign of current vector rotation: positive for counterclockwise (ccw) rotating and negative for clockwise (cw) rotating currents. The technique involves the decomposition of the velocity vector into cw and ccw rotating circular complex-valued components. First, a rotary spectral analysis was performed to identify the dominant frequencies f and to quantify the energy $S(f)$ of current velocity variability. Both cw S_- (negative) and ccw S_+ (positive) power spectra revealed pronounced peaks at the semi-diurnal frequency. After that, using these peak values, the rotary coefficient $r = (S_+ - S_-)/(S_+ + S_-)$ was estimated at every grid point. r ranges from -1 for clockwise motion to $+1$ for counter-clockwise motion ($r = 0$ is oscillating non-rotational flow). The corresponding sign of r (positive or negative) was assigned to PCA-derived tidal current ellipses.

Following a guideline proposed by EMEC [14], the major parameters of the tidal flow conventionally used for tidal energy site screening were estimated. In addition to synthetic properties of tidal current ellipses, statistical estimates of tidal flow such as: the mean velocity over the study period and cumulated occurrence of velocity distribution were provided. The maximum sustained velocity was also documented. This establishes design loads on device support structures and foundations. The tidal flow asymmetry which basically concerns the asymmetry of velocity magnitude was quantified. It represents the imbalance between the strength of flood and ebb current speeds. The current velocity asymmetry coefficient a is defined as follows: $a = \langle V \rangle_{flood} / \langle V \rangle_{ebb}$, where brackets mean time averaging of velocity values on flood and ebb flow respectively. In addition to a , the direction asymmetry $\Delta\theta$ was estimated as $\Delta\theta = |\theta_{flood} - \theta_{ebb} - 180^\circ|$ [13]. This parameter accounts for a deviation of the flow from a straight line, usually associated with the dominant current direction. VHFR velocity measurements provided a unique opportunity of mapping the major properties of the tidal flow required in tidal energy projects.

However, VHFR allows assessing only the surface current velocity (until 0.25 m depth). The knowledge of the vertical structure of current velocity is of primary importance for quantifying the power available at tidal energy sites, especially near the bottom, where the majority of tidal turbines are deployed. Friction effects impact the flow in the bottom layer and the resulting velocity profile can be characterized by a power law: $V(z) = V_0 (z/d)^{1/\alpha}$ [37]. V_0 is the surface velocity, d is the bottom depth, z is the distance above the seabed, and α is an empirical coefficient estimated from linear regression fit of LogLog representation of velocity.

2.6. Theoretical and practical power estimates

The estimation of power density P is required for tidal flow resource assessment at a site. It is defined as: $P = 0.5\rho V^3$, where ρ is the seawater density and V is the horizontal velocity magnitude. Since the power density varies with the cube of velocity, the time-mean power density cannot be obtained by simply substituting the mean current speed into the above power density equation. Once the time variation of velocities is known for each point of the regular grid, the distribution of power densities can be readily calculated and averaged to find the time mean power density [38]. Estimation of the vertical structure of current velocity allows to evaluate the power available at different levels of the water column.

Following the methodology proposed by Blunden and Bahaj [39], the practical power $P_p = 0.5\rho C_p S V^3$ was estimated considering a single rotor MCT SeaGen turbine. Here, S is the swept area of the turbine, the cut-in speed is set to 1 m/s and the drive train rates at 600 kW for current velocity higher than 2.5 m/s. First, a single turbine (16 m diameter D) was assumed to

operate in top half of the water column where tidal currents are the strongest. Then, an array of 32 turbines, arranged in two rows in an area of 1 km², facing the principal flow direction, was used for estimating the practically extractable power. Lateral and row spacing of the turbines were set to 3D and 30D respectively, as in [39], and a row-wise attenuation factor, set to 0.9, was applied to decrease the incident flow on the second row. A conservative uniform power coefficient $C_p = 0.35$ was assumed instead of SeaGen power curve [40,41]. Using these two configurations, the monthly mean practical power was estimated.

3. Results

3.1. Tidal current velocity

The parameters of synthesized tidal current ellipses used to quantify spatial variability of tidal currents derived from PCA are shown in Fig. 2 for 16 May. During this day, the strongest currents of spring tide were observed. Ellipse orientation shows that the current is strongly controlled by the topography, producing alignment of the major axes along the depth contours. An anisotropy in current field with a relatively high ellipticity is observed over the sandbanks, in the middle of the study domain.

White and black ellipses in Fig. 2 indicate that the current are rotating clockwise (cw) and counter-clockwise (ccw) respectively. Two distinct zones with opposite sign of rotation of the tidal current vector are clearly identified. They are separated by a line roughly following the 30-m isobath. It suggests that along this line, tidal motion produces alternatively divergent and convergent surface current vector during certain periods of the tidal cycle.

The time averaged current velocity distribution shows low spatial variations with values ranging from 0.5 to 1 m/s, with the highest velocity value observed off the Cape GN. The maximum surface current speed observed by the radars is higher than 2 m/s in the entire study area.

3.2. Exceedance probability of velocity

In tidal energy projects, it is customary to calculate the exceedance probability of velocity distribution: the percentage time of a specified current speed exceeded. Fig. 3 shows spatial distribution of the percentage time of the current velocities

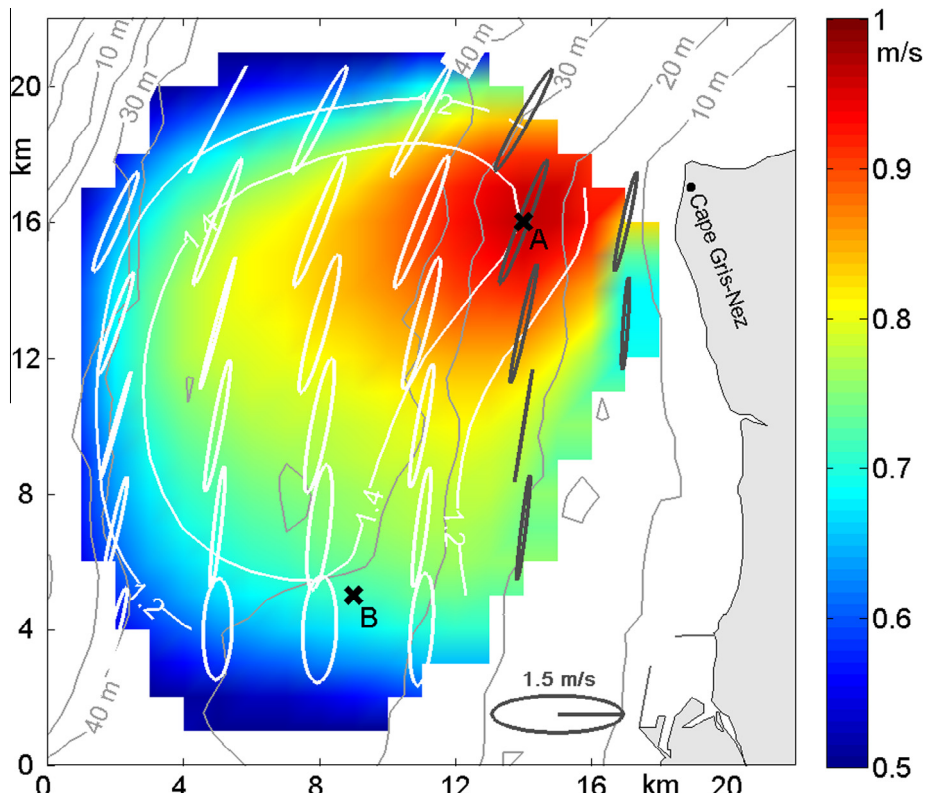


Fig. 2. Mean surface current velocity during the whole study period (color shading) and during the spring tide period in May 2003 (white contours). Shown also tidal current ellipses derived from PCA on May 16, 2003 (every third ellipse is shown). Black ellipses denote counter-clockwise rotating tidal currents and white ellipses denote clockwise rotating currents. Black crosses show locations selected for detailed analysis.

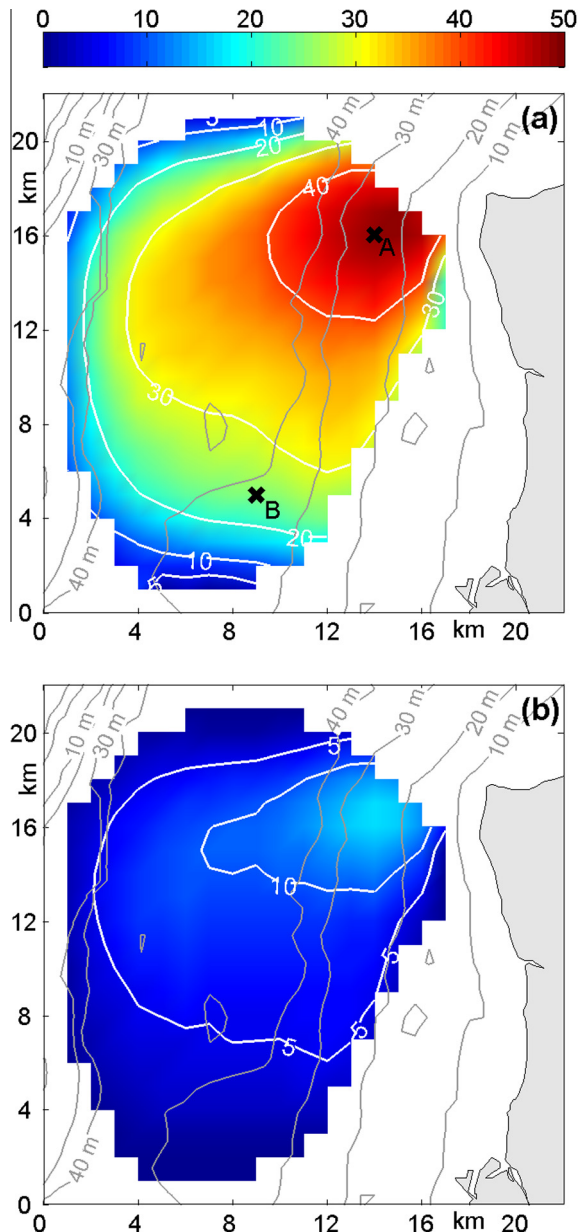


Fig. 3. Percentage time current velocities are exceeded: 1.0 m/s (a), 1.5 m/s (b).

of 1 m/s and 1.5 m/s exceeded during the period of observations. Globally, the velocity value of 1 m/s is reached in the majority of the domain with a minimum occurrence of 20%. In the central part, this velocity was exceeded 30% of time and in the northeastern sector, 50% of time. Spatial distribution of the occurrence velocity value of 1.5 m/s shows smaller range of variations: from 5 to 15% of time in the majority of the area. The peak occurrence is reached in the northeastern sector (Fig. 3(b)).

Velocity histograms provide a simple way to evaluate the available resource at any point of a site. They indicate what percentage of time could be used for power generation. Fig. 4 shows the cumulated occurrence of tidal current velocity observed in two locations selected for detailed analysis: point A located westward of the Cape GN and point B located westward of the BLH (see Fig. 3(a) for locations). The velocity of 1 m/s is exceeded 50% of time in location A and 25% of time in location B. The current speed of 1.5 m/s is exceeded 3 times more often in A than in B (respectively 18% and 6% of time). The mean current velocity is found to be 1 m/s in A and 0.75 m/s in B. This difference results from the change in flow regime. The strait narrowing and the presence of Cape GN cause flow acceleration and provides the highest tidal current velocity there.

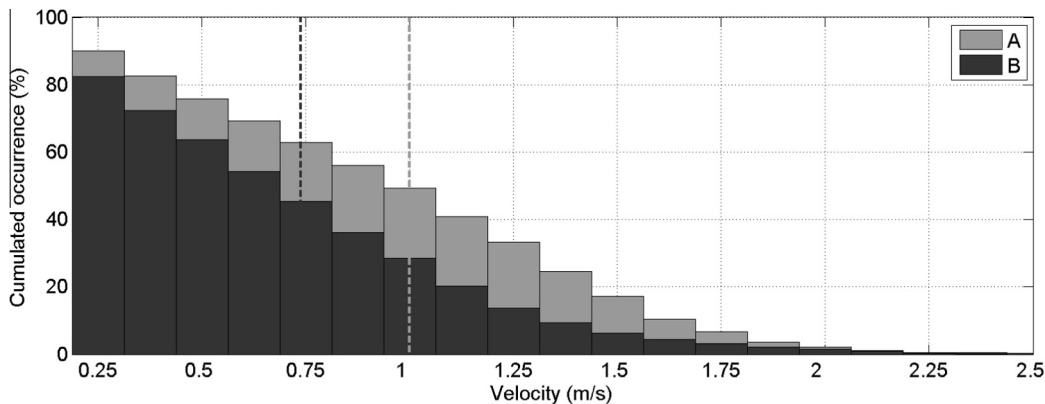


Fig. 4. Cumulative occurrence of velocity magnitude in locations A and B (see Fig. 3(a) for locations). Dashed lines represent the mean velocity at each location.

3.3. Flow asymmetry

Tidal flow asymmetry basically concerns the asymmetry of velocity magnitude. A strong imbalance between the strength of flood and ebb current speeds can exist thus generating asymmetry in power extraction and reducing the overall energy yield [10].

The current asymmetry a is found higher than 1 in almost whole study domain (Fig. 5), indicating the flood flow dominance. The only exception is the eastern part of the area where the asymmetry is slightly less than 1. The maximum current asymmetry ($a = 1.6$) is observed 6 km westward of the Cape GN, indicating the effect of cape on spatial distribution of phase and amplitude of the principal (M_2) tidal constituent and its higher order harmonics (M_4, MS_4) [42].

3.4. Direction asymmetry

Current direction is a relevant metric for tidal stream energy conversion as the predominant design concept for energy converter is that of a fixed horizontal axis turbine. The performance of such energy generating system is degraded if the current direction and rotor plane are misaligned. The asymmetry $\Delta\theta$ between the principal direction of ebb and flood flows varies from 2° to 10° (Fig. 6). The minimum asymmetry is observed in the southern part of the domain. $\Delta\theta$ gradually increases until 10° in the northern part, where the maximum current occurs (Fig. 2). There, on ebb tide, the tidal wave arriving from the North Sea has the southwest direction. On flood flow, tidal wave propagates northward generating a significant misalignment in current direction.

3.5. Velocity profiles

Knowledge on the vertical variation of flow velocity is a critical component of tidal energy resource assessment. Velocity profiles provided by ADCP measurements performed off the BLH, were analyzed for different stages of the tidal cycle: peak velocity period, flood and ebb flow period preceding and following the peak velocity. The time interval used for analysis was set to one hour for each tidal stage. The velocity profiles recorded during multiple 1-h intervals were considered for each of the three tidal stages encountering the peak velocity. Fig. 7 shows the time averaged velocity profiles observed during flood and ebb tidal flow. Based on the data acquired in 2008 and 2009, the vertical profile was found following the 1/6th law on flood tide and the 1/7th law on ebb tide. The analysis also shows that lower value of α is achieved one hour before the peak velocity. Then, it gradually increases until the maximum value, reached one hour after the peak velocity (Table 1). Moreover, α shows larger variation on ebb tide than on flood tide with values ranging from 6 to 7.5 and 5.5 to 6.5 respectively (Table 1). The mean error of α estimation (standard deviation $\Delta\alpha$) for each 1 h long period of tidal flow was found close to 1.

Following the same methodology, velocity profiles from numerical modeling were analyzed and compared with profiles from ADCP measurements in June 2009. The model simulates velocity distribution in the whole water column, including the surface layer. There, ADCP does not provide reliable velocity measurements. Only an extrapolation allows approximating the velocity distribution in the uppermost surface layer. Fig. 7 shows the velocity profiles obtained from the model and from the ADCP measurements. The extrapolated velocity profiles in the surface layer are consistent with that simulated by the model. Power law parameter α is in a very good agreement for modeled and observed profiles with relative error not exceeding 7%. The shape of velocity profiles generated by the model for different stage of tidal cycle shows low variation with providing the standard deviation $\Delta\alpha = 0.3$ on average (Table 1).

Velocities recorded by ADCP and modeled velocity time series were also compared. Fig. 8 shows that the measured and modeled velocities are in phase, the fortnight variation and diurnal inequality of current velocity are accurately reproduced.

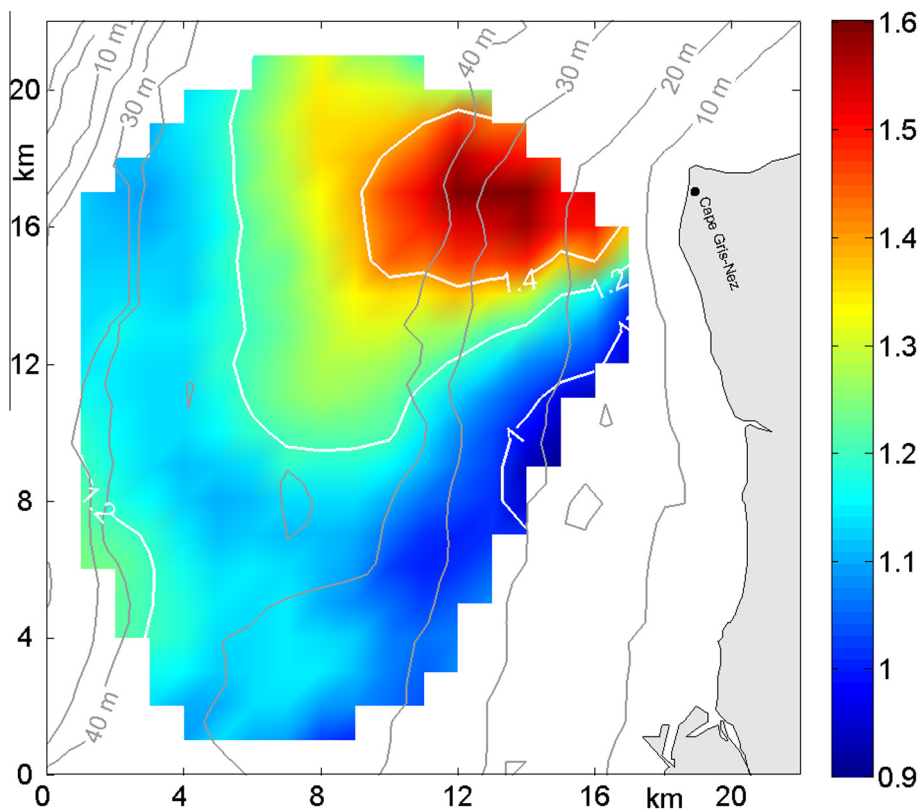


Fig. 5. Current velocity asymmetry a distribution.

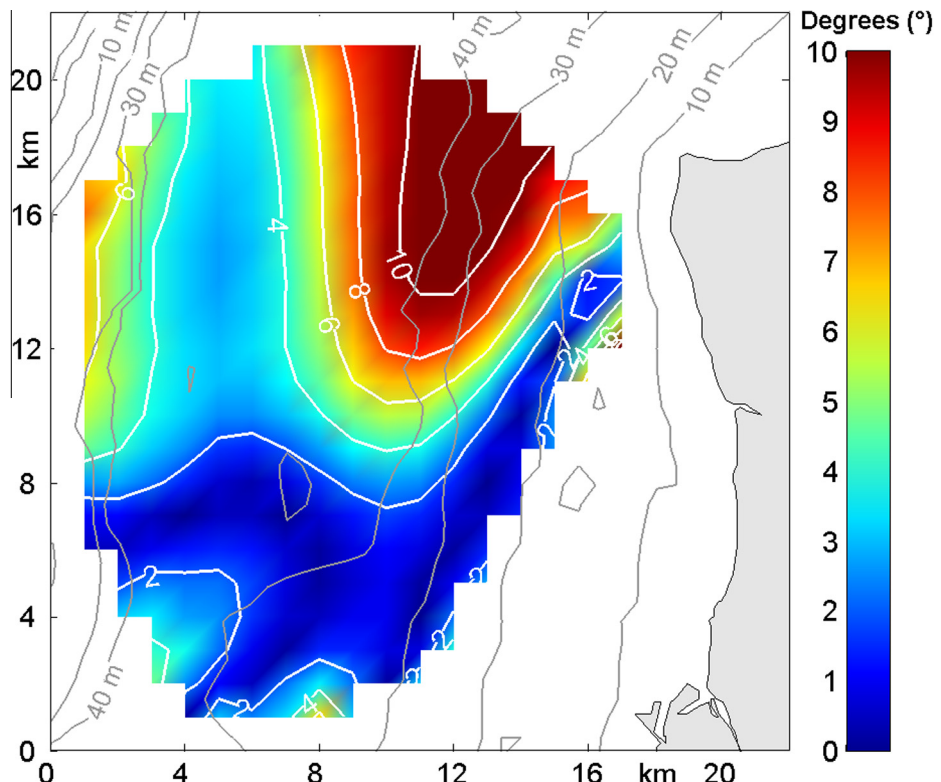


Fig. 6. Direction asymmetry $\Delta\theta$ (deg) between ebb and flood tide flow.

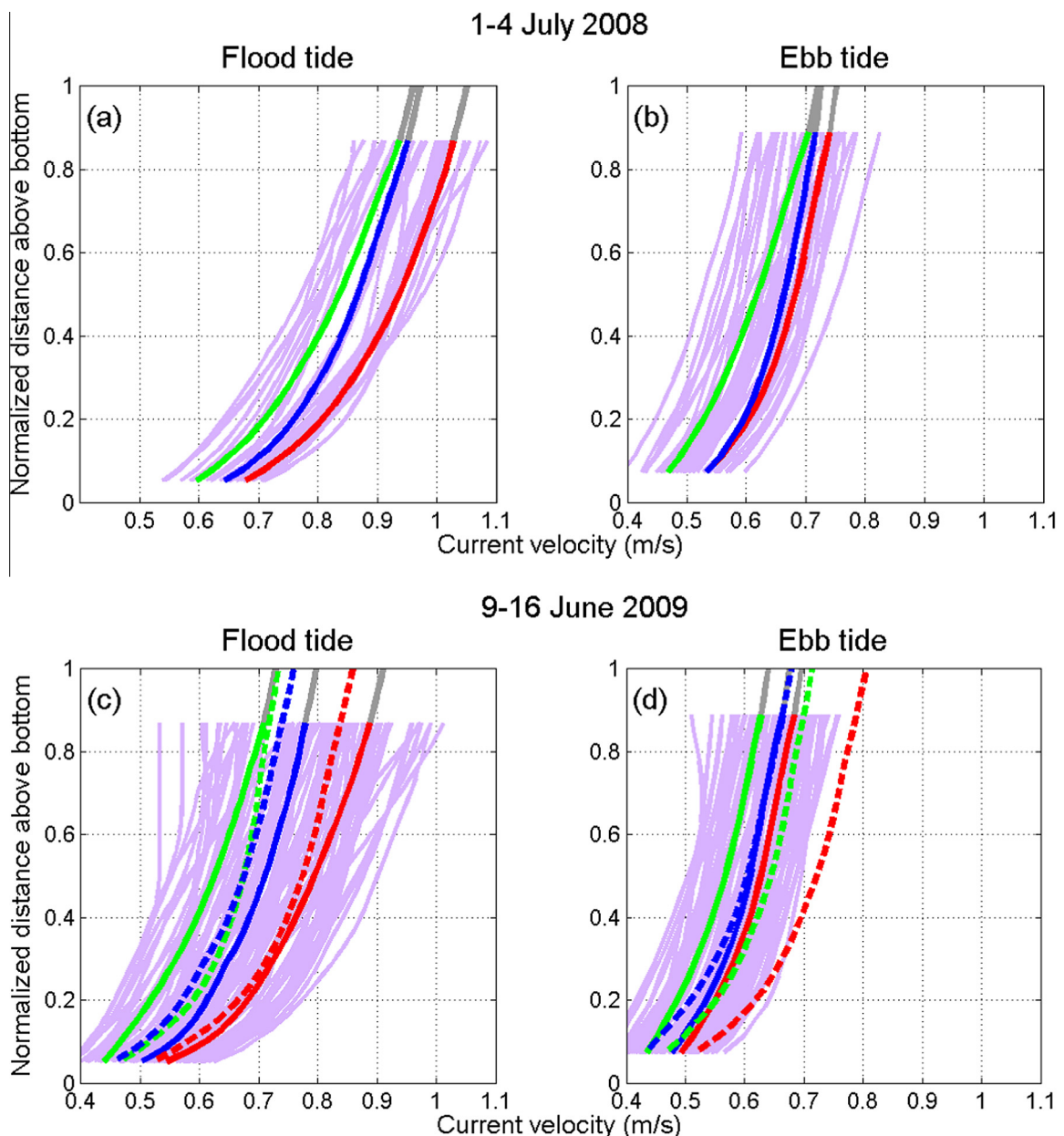


Fig. 7. Current velocity profiles during flood and ebb tide flow derived from ADCP measurements in 2008 (a-b) and in 2009 (c-d). Mean velocity profiles during the peak current are shown in red (one hour averaging period is centered on peak velocity). One hour averaged velocity profiles observed one hour before and one hour after the peak velocity are given in green and blue respectively. Velocity profiles provided by ADCP (20-min averaged) are given in mauve. Only profiles with depth averaged velocity >0.5 m/s are shown. Color solid and dashed lines match observed and modeled velocity profiles. Profile extrapolation to surface is shown in grey.

Table 1

Power coefficient α of the velocity profiles approximated by the power law for three specific periods of current evolution in the vicinity of a peak current, for flood and ebb tide. Power coefficient standard deviation $\Delta\alpha$ is estimated using individual 20-min averaged profiles derived from ADCP measurements and numerical model.

		Peak vel. – 1 h	Peak vel.	Peak vel. +1 h	$\langle \alpha \rangle$	$\Delta\alpha$
Flood	ADCP	5.6	6.1	6.5	6	1.1
	MODEL	5.6	6.2	6.7	6.1	0.3
Ebb	ADCP	6.0	7.1	7.5	6.9	1
	MODEL	6.2	7.4	7.6	7	0.2

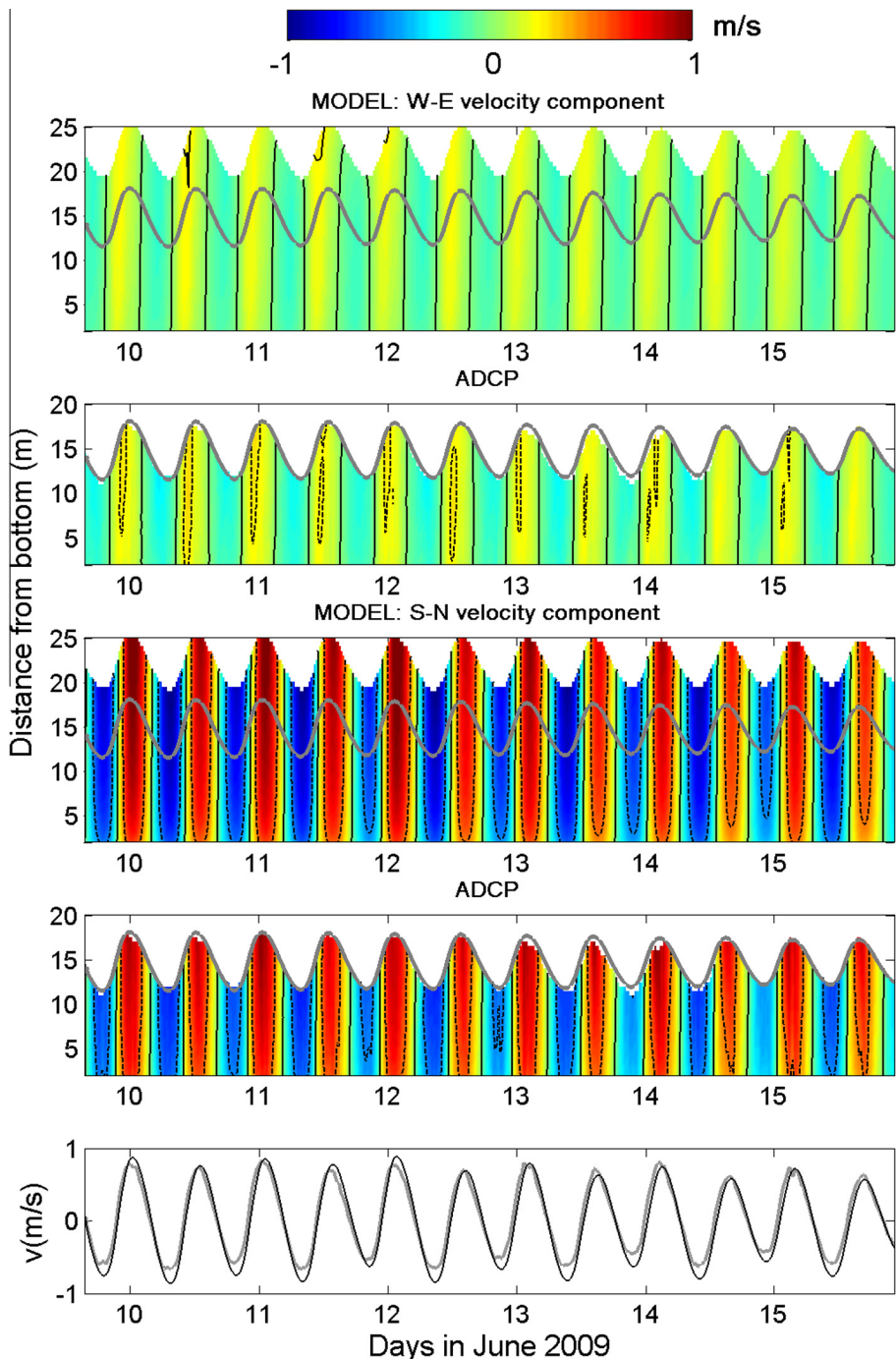


Fig. 8. Time-depth variability of cross-shore current velocity u from the model and ADCP measurements (two upper panels) and along-shore velocity v (panels three and four), during one week period in June 2009. Grey curve represents the upper limit of ADCP measurements. Lower panel shows time series of the depth-averaged along-shore velocity component given by ADCP (grey) and the model (black).

The agreement with observations is better for the meridional (along-shore) velocity component than for zonal (cross-shore) component. Moreover, the model overestimates the current velocity magnitude by 20% during ebb tide, whereas during flood tide the agreement is excellent (discrepancy is 1%). Fig. 9 represents histograms of cumulative occurrence of velocity magnitude provided both by the model and by observations. On average, the model velocities are slightly overestimated (by 5%) with the exception of very low velocities (<0.35 m/s). For this range, the modeled velocities are lower than observed velocities.

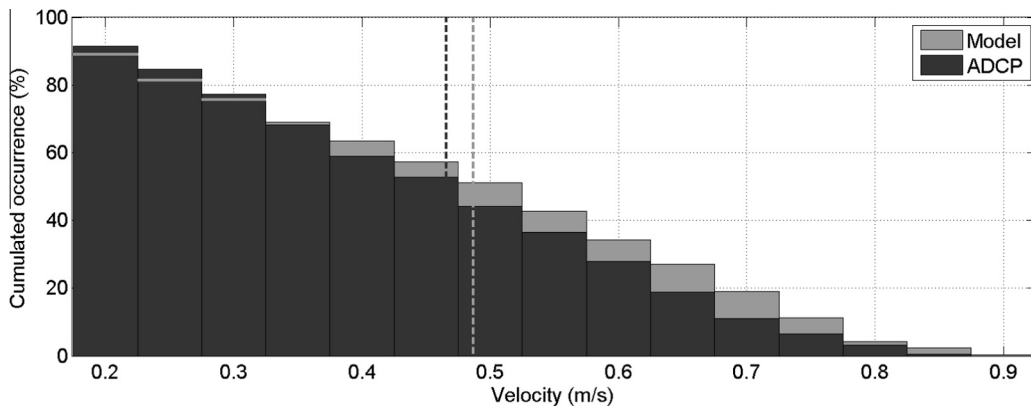


Fig. 9. Cumulative occurrence of measured by ADCP (black) and modeled (grey) velocities in ADCP location (see Fig. 1 for ADCP location). Grey and black dashed lines match mean velocity values.

Table 2

Relative error ε (%) of ADCP velocity profile approximation by the power law $V(z) = \langle V \rangle (z/K_0 d)^{1/2}$ for four values of bed roughness coefficient: $K_0 = 0.2, 0.3, 0.4$ and 0.5 mm, and for three tidal stages encountering the peak velocity.

K_0 (mm)	Peak vel. -1 h	Peak vel.	Peak vel. $+1$ h
0.2	15	13	12
0.3	8	7	6
0.4	3	3	2
0.5	3	3	2

The vertical variation of tidal current velocities can be reconstructed at any grid point of the radar coverage zone by assuming the power law approximation of velocity profiles $V(z)$ derived from ADCP measurements. However, this suggests a strong assumption: the shape of velocity variation with depth is representative for the whole study domain. This hypothesis does not account for sea bottom roughness variation in the Dover Strait, where sand and gravel bottom types are common.

A bottom drag coefficient K_0 can be introduced in the power law expression in order to account for sea-bed roughness: $V(z) = \langle V \rangle (z/K_0 d)^{1/2}$, with $\langle V \rangle$ being the depth-averaged velocity and d is the total depth [37]. With two degrees of freedom, the resulting approximation of the velocity profiles $V(z)$ could be different, which can affect the power estimate. To evaluate the impact of sea-bed roughness on the velocity profile shape, the current profiles $V(z)$ were generated using the power law for $K_0 = 0.2, 0.3, 0.4$ and 0.5 mm, covering a large range of bottom types. The ADCP deployment in June 2009 provided the data either side of peak velocity, which are the most important. The discrepancy between the power law approximated and real profiles, estimated in term of the relative error ε , is summarized in Table 2. The best fit ($\varepsilon \sim 2\text{--}3\%$) is achieved for $K_0 = 0.4$ and 0.5 mm, matching the sand/gravel nature of the sea-bed in the Dover Strait. Lower values of K_0 appeared inappropriate. The approximation is found slightly better for tidal current occurring after the peak velocity ($\varepsilon \sim 2\%$).

Current profile approximation using the surface velocity V_0 revealed the discrepancy ε of 2% for all three stages of current evolution around the peak flow. The comparison ensures a good choice of expression for $V(z)$ and also provides a range of error of velocity approximation, which can affect the power estimate. Variations in bottom roughness coefficient with respect to bottom type do not show a strong effect on the approximation error (for sea-bed nature assumed to be representative in the study area and characterized by $K_0 = 0.4$ and 0.5 mm).

3.6. Tidal stream potential

The kinetic power density is the primary metric used to characterize the theoretical potential and its spatial variation at a site. It is possible to evaluate the available power density at different space and time scales and vertical levels from velocity observations. Most of the tidal turbines are designed for deployment on the sea floor (e.g. Open Hydro, Sabella) but some of them (e.g. Hydro-Gen, Evopod by Oceanflow) are installed in the surface layer to take advantage of the highest current velocities. For this reason, the power density should be estimated for different altitudes according to device's deployment level.

The radar observations provide information about spatial and temporal variability of surface currents. In addition, it is assumed that the ADCP-derived velocity profiles are representative for ebb and flood flow at each grid point within the study domain. By merging these two sources of data, the power density time series in the surface and bottom layers (upper and

lower half of the water column) were generated. In this calculation, it was assumed that the vertical variation of the current velocity follows the 1/6th and the 1/7th power law on flood and ebb flow respectively.

As the only variable parameter governing the power is the current velocity, thus, it is not surprising to find similar spatial patterns for both mean tidal current velocity and mean kinetic power density distribution (color shading in Figs. 2 and 10). In the surface layer (Fig. 10a), the mean power density attains its maximum value (0.9 kW/m^2) in the northeastern sector, with peak value of 5 kW/m^2 . For the rest of the study domain, the mean available power is much lower and varies in the range $0.1\text{--}0.6 \text{ kW/m}^2$. In the bottom layer (Fig. 10b), the maximum value of the mean power (0.3 kW/m^2) is also found in the northeastern sector. On average, the kinetic power available in the bottom layer is 3 times lower than that available in the surface layer. During spring tide, the power in the tidal flow increases considerably and attains 2.2 kW/m^2 and 0.7 kW/m^2 in the surface and bottom layers respectively, in the northeastern sector.

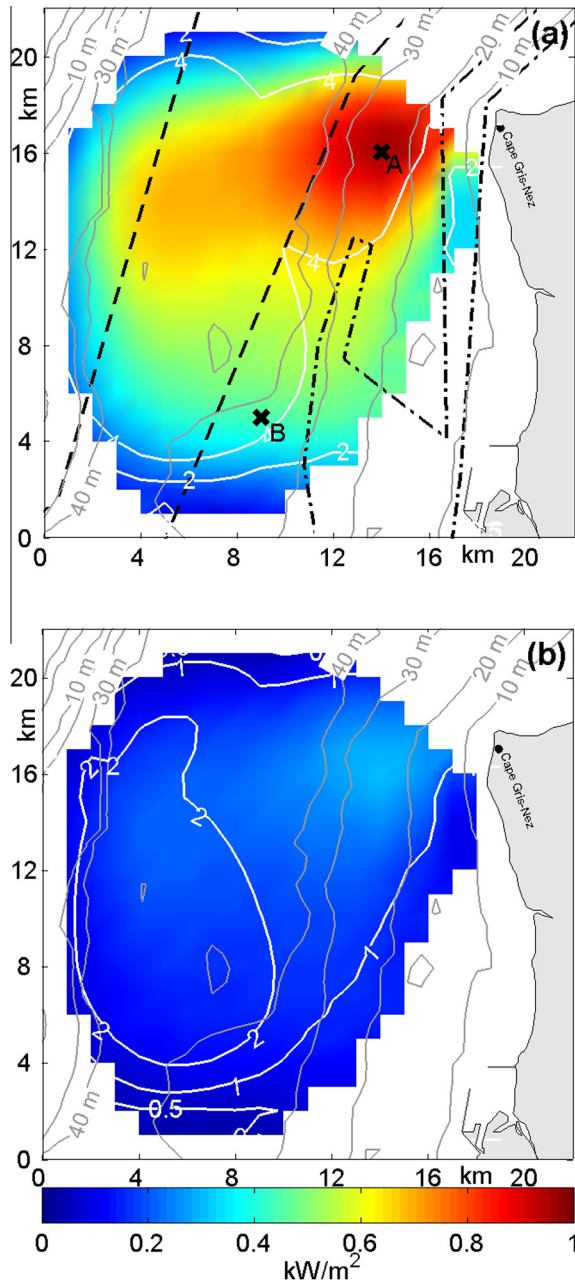


Fig. 10. Maximum (white contours) and time averaged (color shading) kinetic power density available in the surface (a) and bottom (b) layers during the period of radar observations (May 2003). The navigation way of vessels travelling northward and the main fishing area are shown by black dashed and dash-dot lines respectively.

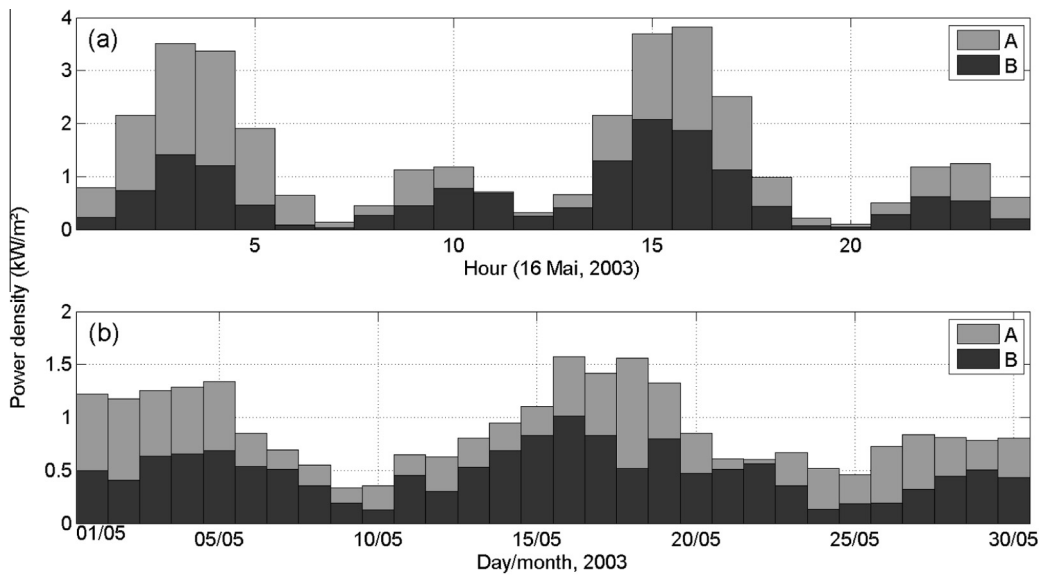


Fig. 11. Hourly (a) and daily (b) values of power density in the surface layer in location A (grey) and B (black).

[Fig. 11](#) represents time series of hourly and daily mean power density values for two geographic locations. At time scale of a day, a semi-diurnal variability and a pronounced inequality of kinetic power are observed in the surface and bottom layers. The latter is caused by current asymmetry – stronger in location A ($a = 1.6$) than in location B ($a = 1.1$). Peak power during flood tide in location A and B, is respectively 3 and 2 times higher than that during ebb tide. For a month long period, a fortnight modulation of power is observed ([Fig. 11b](#)) and two spring tide periods are identified. For mean spring tide conditions, the theoretical power in location A was estimated to be 1.15 kW/m^2 (secondary spring tide) and 1.5 kW/m^2 (primary spring tide). In location B, these respective values are 0.5 kW/m^2 and 1.2 kW/m^2 respectively. On average, the monthly mean power available in location A exceeds that in location B by a factor of two (0.9 kW/m^2 and 0.5 kW/m^2 respectively).

The practically extractable power P_p was estimated in location A for two configurations: a single tidal turbine and an array of turbines deployed over an area of 1 km^2 ([Section 2.6](#)). The water depth is around 25 m there and the mean spring tide velocity is 1.4 m/s , thus providing favorable conditions for tidal energy conversion. The monthly mean practical power values were found to be: $\sim 0.1 \text{ GWh}$ for a single device and $\sim 2.5 \text{ GWh/km}^2$ for an array.

4. Discussion and conclusions

Assessment of the available tidal stream resource is an essential first step toward successful site selection, device deployment, and further exploitation of the resource [[4](#)]. However site selection is not simply a case of identifying regions with large tidal currents. Instead, resource assessment and site selection should consider a wide range of factors, including temporal and spatial variability of the resource and tidal flow parameters, such as current asymmetry, change in phase, velocity profile, ... (e.g. [[10](#)]). Detailed observational campaigns are not sufficient (or too much expensive) at the scale required for detailed resource characterization. Therefore, tidal-stream resource assessments typically make extensive use of validated hydrodynamic models (e.g. [[43](#)]).

In our study, we present a novel approach for resource assessment based on observations of tidal flow dynamics by oceanographic radars in combination with ADCP measurements. The method can be applied separately or in conjunction with numerical modeling for analysis of tidal stream potential at different sites. It was recently used at a highly energetic site in the Iroise Sea [[26](#)] where French turbine Sabella D10 is deployed since 2015.

Two VHFR were installed in 2003 on the Opal coast of France, in the Dover Strait for monitoring surface circulation and assessing processes governing the marine system dynamics in the eastern English Channel. The radars provided a 35-day long dataset of surface current velocities over an area of 500 km^2 . Using advantages of the radar technology (spatial coverage, high resolution, continuous data acquisition, ...) the remotely sensed velocities were used for assessing the resource, quantifying the major metrics of a tidal flow and their space and time variation. Radar derived surface velocities were supplemented by ADCP measurements performed in the radar coverage zone, 6 km offshore the BLH. This allowed quantifying spatial and temporal variability of the tidal energy potential in three dimensions. A 3D numerical model was also used to generate velocity time series and to compare them with velocities provided by both VHFR and ADCP. The comparison revealed a very good agreement thus allowing the use of an extensively validated regional numerical model for assessing tidal stream resource in different sectors of the Channel.

Up to date the Dover Strait was considered as a promising site for tidal stream energy conversion [2]. However there is no reliable estimate of a technically exploitable potential in this area. The present study allowed a complete site screening and resource quantification in the French sector of the Dover Strait. The area of high potential is found westward of the Cape GN. There, the mean tidal current velocity is 1 m/s, spring tide velocity is close to 1.4 m/s, and peak velocity is 2.5 m/s. The velocity of 1 m/s is exceeded 50% of time. The strait narrowing and the presence of Cape GN affect considerably the tidal flow, cause the flow acceleration and also flow misalignment between flood and ebb tide. The mean ebb/flood flow direction asymmetry is found to be 10° west of the Cape GN. This low value of asymmetry might result in a big imbalance of power production. Using a numerical model, Frost et al. [44] performed an assessment of the impact of non-rectilinear flows on turbine rotor performance. They focused on estimating the coefficient of power C_p defined as the ratio of power retrieved by the turbine to the maximum available power from the flow incoming through the rotor area. The authors showed that an axial flow misalignment $\Delta\theta$ of 10° to 20° results in a 7.5–29% reduction in peak C_p respectively.

Another tidal flow property which considerably affects the power production is the current asymmetry resulting in a distortion of the tidal velocity curve and following flood or ebb dominance of the flow regime. In the study area, the majority of the domain is flood dominated ($a > 1$) with the maximum asymmetry value ($a = 1.6$) reached in the northeastern part of the area (Fig. 5). The distortion of the tide is caused by a non-linear growth of compound tidal constituents [45]. Pingree and Griffiths [46] showed that the interaction of the principal semi-diurnal tidal constituent M_2 and its first harmonic M_4 explains the general features of observed tidal asymmetries. The tidal current amplitude of M_4 relative to that of M_2 appears particularly high over shallow water continental shelf region. Moreover, Speer and Aubrey [47] demonstrated that the current asymmetry is dependent on a relationship between the phase of M_2 and M_4 . The maximum asymmetry is achieved when the phase of M_2 is two times bigger than that of M_4 . Thiébaut and Sentchev [26] showed that in the Fromveur Strait, the spatial distribution of M_2 and M_4 phases are such that the current asymmetry varies in a wide range: from 0.5 to 2.5, generating high current velocity variation between flood and ebb tide. Numerical simulations performed by Jouanneau et al. [29] revealed significant amplitude of M_4 in the eastern English Channel generating a high asymmetry of the sea surface height there.

The tidal current asymmetry can generate a strong variability of power production over a day thus reducing the overall energy yield. Neill et al. [10], estimated the power output of the 1.2 MW twin-rotor MCT SeaGen turbine hypothetically installed in a highly energetic tidal channel in Orkney. The authors considered two locations of opposite asymmetry: an ebb-dominant site ($a = 0.75$) and a flood-dominant site ($a = 1.35$). In the latter case, the peak power generated during spring flood flow was four times bigger than that generated during ebb tide.

A high asymmetry of the tidal flow in the Dover Strait (up to 1.6) can cause a high imbalance in power production. Our estimations showed that in the vicinity of the Cape GN, where the strongest current occurs (location A), the mean power in the surface layer during spring flood flow is close to 2.2 kW/m², whereas it is three times lower during ebb tide.

Moreover, current velocities or sea surface elevation are not the only variables affected by the tidal asymmetry. Turbulent properties, considered as critical components of tidal energy resource assessment are also impacted [20,21].

Regarding the velocity variation with depth, it was shown that the velocity profiles follow a power law with power coefficient α ranging from 6 to 7.5 and from 5.5 to 6.5 for ebb and flood tide respectively. The lowest value of α is achieved one hour before the peak velocity and the highest is reached one hour after the maximum current occurred. Numerical simulations of tidal current velocities for the period of ADCP deployment showed a very good overall agreement with measurements and also in determination of α . On average, the numerical model overestimates the power coefficient α by only 7%, with the value of standard deviation five times lower than that provided by measurements. Although the model is forced by realistic winds and tide, it cannot take into account all specific or extreme conditions occurred during the ADCP deployment. The wind measurements revealed calm and stormy weather conditions followed each other during the ADCP deployment. During storm, winds with magnitude of 15 m/s and significant wave height up to 1.4 m were observed. Analysis of velocity time series recorded by ADCP revealed a noticeable contribution of wind-induced waves to spectral structure of velocity fluctuations in the surface layer [48]. This provides an explanation of higher variance in determination of α from the experimental data.

ADCP measurements allow to project space-time variations of surface current velocities on different depth levels and thus enable the hydro-kinetic power reconstruction at different altitudes. A combination of expressions for available power P and for velocity profile $V(z)$ provides an expression for power variation with depth and time: $P(z,t) = 0.5\rho V_0(t)^3(z/d)^{3/\alpha}$. Thus radar measurements of surface velocity $V_0(t)$ can be used to assess power variations at different space and time scales and at different vertical levels.

The mean kinetic power $\langle P \rangle$ was estimated at different spatial locations in the surface and bottom layers. The maximum value (0.9 kW/m²) of the monthly mean power is found in the surface layer in location A, west of the Cape GN. During spring tide, the mean power varies from 0.7 kW/m² on ebb to 2.2 kW/m² on flood flow there. For comparison, the mean kinetic power in a highly energetic sector of the Alderney Race is of the order of 14 kW/m² [49]. In the Fromveur Strait (Western Britanny), Thiébaut and Sentchev [26] documented the mean power level of 5.5 kW/m². Regarding these resource assessments, it appears that the power available in the Dover Strait (location A) is low but not dramatically lower than that estimated at other sites considered as promising in European seas [12]. The power available in the bottom layer was found three times lower than that in the surface layer. This is related to the bottom friction affecting the flow and resulting in vertical variation of the velocity which follows the power law.

The practical power which could be generated in the Dover Strait by an array of single rotor SeaGen current turbines was assessed for two configurations and compared with similar estimates performed by Blunden and Bahaj [39] in the Alas Strait, Indonesia. The authors carried out the power estimation using a 3D hydrodynamic numerical model of the Indonesia seas. An array of single rotor SeaGen turbines was assumed to be installed over an area of approximately 14 km^2 (depth $<40 \text{ m}$), and each sub-area of 0.75 km^2 comprised 16–28 turbines (a maximum of 32 turbines per km^2). The total monthly mean practical power was estimated to be 27.5 GWh, thus providing 2 GWh per km^2 .

An array of 32 tidal turbines, virtually installed in an area of 1 km^2 , west of the Cape GN in the Dover Strait, can provide $\sim 2.5 \text{ GWh}$ during a month. This estimate is 20% higher than that obtained in the Alas Strait, for roughly comparable environmental conditions: the depth-averaged spring tide velocity of 1.85 m/s was documented by Blunden and Bahaj [39], and $\sim 2.1 \text{ m/s}$ in the present study. This small difference in velocity appeared amplified in power estimate due to non-linearity. Moreover, taking into the account geographic and environmental constraints in the Dover Strait (Section 2.1), it appears that the total area of high potential suitable for tidal current energy conversion off the Cap GN is approximately 16 km^2 (Fig. 10a), which is also similar to that documented in the Alas Strait. Compared to the maximum extractable power of 1.3 GW in the Johnstone Strait, Canada, reported by Sutherland et al. [9], the tidal flow potential in the Dover Strait can be considered as low.

Velocity time series, averaged in the upper half of the water column, were used in calculations presented above. The average value was derived from the power law approximation of current profiles observed in the Dover Strait. The analysis of ADCP data showed that the mean power profile for flood and ebb tide are sensibly different (Fig. 12). Power variation with depth takes into account the $1/6$ th (flood) and $1/7$ th (ebb) power laws, derived from the statistic analysis of ADCP data, but also the tidal flow asymmetry. At ADCP location, the mean depth-averaged power was estimated to be 0.7 kW/m^2 and 0.25 kW/m^2 on flood and ebb tide respectively, indicating the effect of the current asymmetry. In order to evaluate the impact of α on power estimation, the $1/7$ th and $1/5$ th power laws for velocity profiles were used in estimating the power

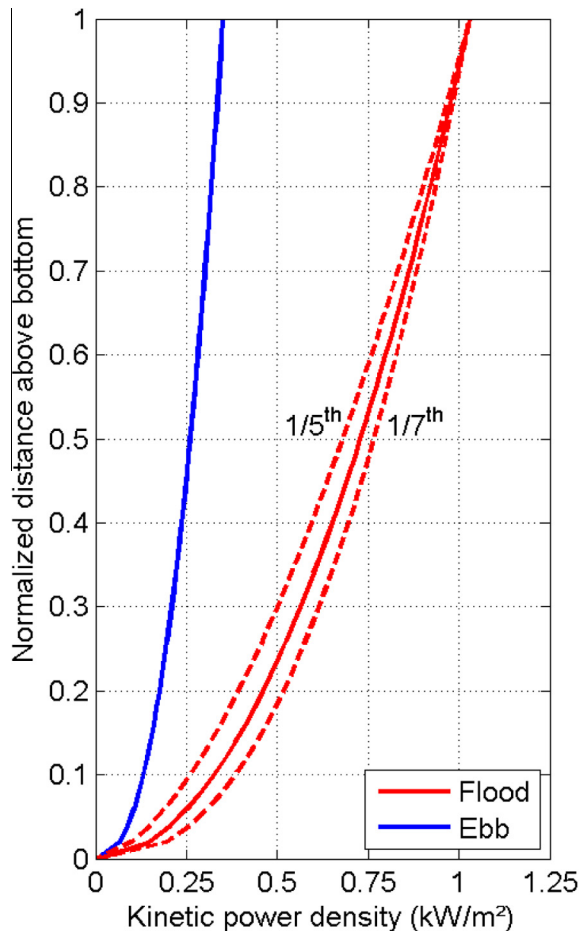


Fig. 12. Vertical profile of the mean kinetic power density in location A obtained by averaging the velocity profiles approximated by the $1/7$ th power law on ebb flow and by the $1/6$ th power law on flood flow. Dashed lines show the mean power profile on flood tide derived from velocity approximation by the $1/5$ th and $1/7$ th power law (i.e. $\pm\Delta\alpha$).

P during flood tide (dashed lines in Fig. 12). The resulted depth-averaged power changed by ~6%. On the contrary, the discrepancy increases to ~11% for power available in the bottom layer (lower half of the water column).

A variation in bottom friction due to change of the bottom floor nature (sand, gravel, ...) may affect the shape of velocity distribution with depth. It was found that a change in bottom roughness coefficient K_0 produces a velocity variation of the order of 2–3% in the bottom layer. The resulting variation in theoretical power estimate (<9%) is roughly comparable with that caused by the variation of power law coefficient α within the range of observed variability.

In summary, surface velocity time series recorded by VHF radars in the Dover Strait were used in combination with ADCP measurements for assessing and mapping the tidal stream resource and for quantifying the major metrics of the tidal flow required for detailed resource characterization. The observations revealed a large spatial and temporal variability of tidal stream and power density, an important asymmetry of tidal currents causing a large imbalance of power production during ebb and flood flow. The vertical profile of power density was reconstructed and used for quantifying the amount of power available in the bottom and surface layers at different time and space scales. The data analysis showed that the most energetic area is located west of the Cape Gris Nez, outside the northward navigation way and fishing area. Velocities exceeding 1 m/s are observed more than 50% of time there and the spring tide velocity is of the order of 1.4 m/s. This provides the temporal mean power density of 0.9 kW/m² in the surface layer and 0.3 kW/m² in the bottom layer. The level of energy available in the flow is assumed sufficient for potential future technology testing in this area.

An extensively validated regional numerical model MARS-3D was used to generate velocity time series and to compare them with observed velocities. The comparison revealed a very good agreement thus allowing the use of the model for assessing tidal stream resource in extended area in the eastern English Channel.

Acknowledgments

The study was supported by the project PRO-TIDE of the Interreg IVB NW Europe program and represents a contribution to this project. The authors acknowledge funding support by the Pôle Metropolitain de la Côte d'Opale (PMCO).

References

- [1] R.H. Charlier, J.R. Justus, Ocean energies: Environmental, Economic and Technological Aspects of Alternative Power Sources, vol. 56, Elsevier, 1993.
- [2] E.C. Joule II, The Exploitation of Tidal and Marine Currents, Commission of European Communities, London, 1996.
- [3] UK Department, Trade and Industry, Atlas of UK Marine Renewable Energy Resources, 2004 (Technical report).
- [4] L.S. Blunden, A.S. Bahaj, Tidal energy resource assessment for tidal stream generators, Proc. Instit. Mech. Eng., Part A: J. Power Energy 21 (2) (2007) 137–146.
- [5] L. Goddijn-Murphy, D.K. Woolf, M.C. Easton, Current patterns in the inner sound (Pentland Firth) from underway ADCP data*, J. Atmos. Ocean. Technol. 30 (1) (2013) 96–111.
- [6] A. Sentchev, M. Yaremchuk, Monitoring tidal currents with a towed ADCP system, Ocean Dyn. 66 (1) (2016) 119–132.
- [7] L.S. Blunden, A.S. Bahaj, Initial evaluation of tidal stream energy resources at Portland Bill, UK, Renewable Energy 31 (2) (2006) 121–132.
- [8] J. Xia, R.A. Falconer, B. Lin, Numerical model assessment of tidal stream energy resources in the Severn Estuary, UK, Proc. Instit. Mech. Eng., Part A: J. Power Energy 224 (7) (2010) 969–983.
- [9] G. Sutherland, M. Foreman, C. Garrett, Tidal current energy assessment for Johnstone Strait, Vancouver Island, Proc. Instit. Mech. Eng. Part A: J. Power Energy 221 (2) (2007) 147–157.
- [10] S.P. Neill, M.R. Hashemi, M.J. Lewis, The role of tidal asymmetry in characterizing the tidal energy resource of Orkney, Renewable Energy 68 (2014) 337–350.
- [11] M.J. Lewis, S.P. Neill, M.R. Hashemi, M. Reza, Realistic wave conditions and their influence on quantifying the tidal stream energy resource, Appl. Energy 136 (2014) 495–508.
- [12] P.E. Robins, S.P. Neill, M.J. Lewis, S.L. Ward, Characterising the spatial and temporal variability of the tidal-stream energy resource over the northwest European shelf seas, Appl. Energy 147 (2015) 510–522.
- [13] S. Gooch, J. Thomson, B. Polagye, D. Meggitt, Site characterization for tidal power, in: Proceedings of OCEANS 2009, MTS/IEEE Biloxi-Marine Technology for Our Future: Global and Local Challenges, October 2010, IEEE, 1–10.
- [14] C. Legrand, Assessment of Tidal Energy Resource: Marine Renewable Energy Guides, The European Marine Energy Center Ltd (EMEC), London, 2009.
- [15] V. Venugopal, T. Davey, H. Smith, G. Smith, B. Holmes, S. Barrett, J. Lawrence, EquiMar. Deliverable D2. 2. Wave and Tidal Resource Characterisation, 2011.
- [16] W.R. Geyer, R. Signell, Measurements of tidal flow around a headland with a shipboard acoustic Doppler current profiler, J. Geophys. Res.: Oceans 95 (C3) (1990) 3189–3197.
- [17] J.H. Simpson, E.G. Mitchelson-Jacob, A.E. Hill, Flow structure in a channel from an acoustic Doppler current profiler, Cont. Shelf Res. 10 (6) (1990) 589–603.
- [18] R. Vennell, Acoustic Doppler current profiler measurements of tidal phase and amplitude in Cook Strait, New Zealand, Continent. Shelf Res. 14 (4) (1994) 353–364.
- [19] E. Osalus, J. Side, R. Harris, Structure of turbulent flow in EMEC's tidal energy test site, Int. Commun. Heat Mass Transfer 36 (5) (2009) 422–431.
- [20] J. Thomson, B. Polagye, V. Durgesh, M.C. Richmond, Measurements of turbulence at two tidal energy sites in Puget Sound, WA, IEEE J. Oceanic Eng. 37 (3) (2012) 363–374.
- [21] K. Korotenko, A. Sentchev, F.G. Schmitt, N. Jouanneau, Variability of turbulent quantities in the tidal bottom boundary layer: case study in the eastern English Channel, Cont. Shelf Res. 58 (2013) 21–31.
- [22] A. Sentchev, M. Yaremchuk, VHF radar observations of surface currents off the northern Opal coast in the eastern English Channel, Cont. Shelf Res. 27 (19) (2007) 2449–2464.
- [23] P. Broche, J.C. Demaire, P. Forget, Mesure par radar décamétrique cohérent des courants superficiels engendrés par le vent, Oceanol. Acta 6 (1) (1983) 43–53.
- [24] D. Prandle, A new view of near-shore dynamics based on observations from HF radar, Prog. Oceanograph. 27 (3) (1991) 403–438.
- [25] J.D. Paduan, L. Washburn, High-frequency radar observations of ocean surface currents, Annual review of marine science 5 (2013) 115–136.
- [26] M. Thiébaut, A. Sentchev, Estimation of Tidal stream potential in the Iroise Sea from Velocity Observations by High Frequency Radars, Energy Procedia 76 (2015) 17–26.

- [27] A. Sentchev, K. Korotenko, Dispersion processes and transport pattern in the ROFI system of the eastern English Channel derived from a particle-tracking model, *Cont. Shelf Res.* 25 (18) (2005) 2294–2308.
- [28] P.B. du Bois, F. Dumas, L. Solier, C. Voiseux, In-situ database toolbox for short-term dispersion model validation in macro-tidal seas, application for 2D-model, *Cont. Shelf Res.* 36 (2012) 63–82.
- [29] N. Jouanneau, A. Sentchev, F. Dumas, Numerical modelling of circulation and dispersion processes in Boulogne-sur-Mer harbour (Eastern English Channel): sensitivity to physical forcing and harbour design, *Ocean Dyn.* 63 (11–12) (2013) 1321–1340.
- [30] A. Sentchev, M. Yaremchuk, F. Lyard, Residual circulation in the English Channel as a dynamically consistent synthesis of shore-based observations of sea level and currents, *Cont. Shelf Res.* 26 (16) (2006) 1884–1904.
- [31] A. Ouahsine, H. Smaoui, A. Sentchev, Modelling of Tide and Tidally Induced Hydro-Sedimentary Processes in the Eastern Part of the English Channel, *J. Mar. Environ. Eng.* 8 (4) (2006).
- [32] K. Korotenko, A. Sentchev, Study turbulence in shallow tidal coastal zone, *Oceanology* 51 (2011) 1–14.
- [33] S.J. Couch, I. Bryden, Tidal current energy extraction: hydrodynamic resource characteristics, *Proc. Instit. Mech. Eng., Part M: J. Eng. Maritime Environ.* 220 (4) (2006) 185–194.
- [34] P. Lazure, F. Dumas, An external–internal mode coupling for a 3D hydrodynamical model for applications at regional scale (MARS), *Adv. Water Resour.* 31 (2) (2008) 233–250.
- [35] F. Dumas, J.Y. Stanisière, D. Maurer, Hydrodynamic characterization of the Arcachon Bay, using model-derived descriptors, *Cont. Shelf Res.* 29 (8) (2009) 1008–1013.
- [36] R.E. Thomson, W.J. Emery, *Data Analysis Methods in Physical Oceanography*, Newnes, 2014.
- [37] R. Soulsby, *Dynamics of Marine Sands: A Manual for Practical Applications*, Thomas Telford, 1997.
- [38] G. Hagerman, B. Polagye, R. Bedard, M. Previsic, Methodology for estimating tidal current energy resources and power production by tidal in-stream energy conversion (TISEC) devices, EPRI North American tidal in stream power feasibility demonstration project, 1 (2006).
- [39] L.S. Blunden, A.S. Bahaj, N.S. Aziz, Tidal current power for Indonesia? An initial resource estimation for the Alas Strait, *Renewable Energy* 49 (2013) 137–142.
- [40] J. Thake, Development, installation and testing of a large-scale tidal current turbine. Technical report T/06/00210/00/REP, UK Department of Trade and Industry, October 2005.
- [41] W.M.J. Batten, A.S. Bahaj, A.F. Molland, J.R. Chaplin, Hydrodynamics of marine current turbines, *Renewable Energy* 31 (2) (2006) 137–142.
- [42] D. Prandle, Year-long measurements of flow-through the Dover Strait by HF radar and acoustic doppler current profilers (ADCP), *Oceanol. Acta* 16 (5–6) (1993) 457–468.
- [43] M. Lewis, S.P. Neill, P.E. Robins, M.R. Hashemi, Resource assessment for future generations of tidal-stream energy arrays, *Energy* 83 (2015) 403–415.
- [44] C. Frost, P.S. Evans, C.E. Morris, A. Mason-Jones, T. O'Doherty, D. O'Doherty, D., The effect of axial flow misalignment on tidal turbine performance, in: Proceedings of the 1st international conference on renewable energies offshore, 24–26 November 2014.
- [45] D.G. Aubrey, P.E. Speer, A study of non-linear tidal propagation in shallow inlet/estuarine systems Part I: observations, *Estuar. Coast. Shelf Sci.* 21 (2) (1985) 185–205.
- [46] R.D. Pingree, D.K. Griffiths, Sand transport paths around the British Isles resulting from M_2 and M_4 tidal interactions, *J. Mar. Biol. Assoc. United Kingdom* 59 (02) (1979) 497–513.
- [47] P.E. Speer, D.G. Aubrey, A study of non-linear tidal propagation in shallow inlet/estuarine systems Part II: theory, *Estuar. Coast. Shelf Sci.* 21 (2) (1985) 207–224.
- [48] K. Korotenko, A. Sentchev, F.G. Schmitt, Effect of variable winds on current structure and Reynolds stresses in a tidal flow: analysis of experimental data in the eastern English Channel, *Ocean. Sci.* 8 (6) (2012) 1025–1040.
- [49] D.S. Coles, L.S. Blunden, A.S. Bahaj, Energy extraction potential from the Alderney Race, in: Proceedings of the 11th European Wave & Tidal Energy Conference, Nantes, France, 6–11 September 2015.